Time-of-flight spin-echo small-angle neutron scattering applied to biological cell nuclei

Iashina, E.G.; Bouwman, W.G.; Duif, C.P.; Dalgliesh, Robert M.; Varfolomeeva, Elena Y.; Pantina, Rimma A.; Kovalev, Roman A.; Fedorova, Natalia D.; Grigoriev, S. V.

DOI
10.1107/S1600576723007549

Publication date
2023

Document Version
Final published version

Published in
Journal of Applied Crystallography

JOURNAL OF APPLIED CRYSTALLOGRAPHY

ISSN 1600-5767

Time-of-flight spin-echo small-angle neutron scattering applied to biological cell nuclei

Ekaterina G. Iashina,[a,b]* Wim G. Bouwman,[c] Chris P. Duif,[c] Robert Dalgliesh,[d] Elena Y. Varfolomeeva,[b] Rimma A. Pantina,[b] Roman A. Kovalev,[b] Natalia D. Fedorova[b] and Sergey V. Grigoriev[a,b]

[a]Saint Petersburg State University, Ulyanovskaya 1, Saint Petersburg, 198504, Russian Federation, [b]Petersburg Nuclear Physics Institute, NRC 'Kurchatov Institute', Gatchina, Saint Petersburg, 188300, Russian Federation, [c]Delft University of Technology, Mekelweg 15, 2629 JB Delft, The Netherlands, and [d]ISIS Facility, Rutherford Appleton Laboratory, CCLRC, Chilton, Didcot, Oxfordshire OX11 0QX, UK. *Correspondence e-mail: yashina_91@inbox.ru

Received 12 September 2022
Accepted 29 August 2023

Edited by E. P. Gilbert, Australian Centre for Neutron Scattering, ANSTO, Australia

Keywords: time-of-flight spin-echo small-angle neutron scattering; ToF-SESANS; chromatin organization; logarithmic fractals.

The organization of chromatin in the nuclei of rat lymphocyte was studied by time-of-flight spin-echo small-angle neutron scattering (ToF-SESANS). The procedures of the measurements in ToF and monochromatic SESANS modes were compared. It is shown that the sensitivity of the ToF method is significantly higher than that of the monochromatic mode. As a result, the SESANS correlation function can always be extracted from the ToF measurement of polarization, while this is not always the case with the monochromatic mode. The applicability of SESANS to fractal objects at the micrometre scale is demonstrated. The SESANS correlation function is well fitted by the exponential decay $G(z) = \exp(-z/\xi)$ with the correlation length $\xi = 3.7 \pm 0.1$ µm. The exponential decay of the SESANS correlation function can be connected to the logarithmic correlation function $\gamma(r) = \ln(r/\xi)$ and the cubic law of the scattering intensity $I(Q) = Q^{-3}$, which is in agreement with the concept of scattering from fractal objects. This finding is interpreted as evidence of a very specific logarithmic fractal structure of the large-scale organization of chromatin. The model of the logarithmic fractal is visualized as a hierarchical object obeying the volume-conservation principle at different scales.

1. Introduction

One of the most important goals in modern biophysics is the search for the relationship between the structure and the function of biological cell elements. The first step in solving this problem is a precise and full structure definition with the aim of obtaining the most complete spatial picture of the object under study. The small-angle scattering method is one of the most informative techniques for studying the structure of biological molecules at supra-atomic scales from a few nanometres to a few micrometres. The small-angle scattering of X-rays and neutrons allows the study of biological macromolecules under near-native conditions and information to be obtained on their spatial structure (Svergun *et al.*, 2013; Stuhrmann & Miller, 1978; Mahieu & Gabel, 2018; Krueger, 2022).

One of the advantages of small-angle neutron scattering (SANS) is the possibility of applying a contrast technique based on D_2O–H_2O substitution in the solvent, which allows the scattering to be extracted from one of the two parts in a two-component system (Krueger, 2022). This advantage of the SANS technique is often used in investigations of complexes consisting of nucleic acids (NA) and proteins. Standard SANS deals with biological molecules with typical sizes smaller than a few hundred nanometres.

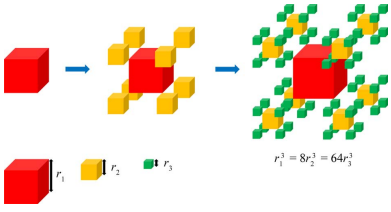

For large biological complexes showing a multiscale hierarchical organization with structural features on the micrometre scale, the standard SANS method is not enough due to its rather high but still limited instrumental resolution. For instance, the existing question of how a very long DNA molecule (sometimes a few metres long) is packed into a relatively small cell nucleus (a few micrometres) (Mirny, 2011; Halverson *et al.*, 2014; Boettiger *et al.*, 2016; Lieberman-Aiden *et al.*, 2009) cannot be answered using only standard SANS – one would also need to use the ultra-small-angle neutron scattering (USANS) techniques that are applicable to the study of matter on the micrometre scale. The spin-echo small-angle neutron scattering (SESANS) method is a relatively new USANS technique to determine the structure of materials in the length range between 20 nm and 20 µm (Rekveldt, 1996; Bouwman *et al.*, 2011; Andersson *et al.*, 2008).

It has recently been shown that SESANS is suitable to study the large-scale organization of chromatin in biological cell nuclei. Chicken erythrocyte nuclei (Lebedev *et al.*, 2005; Iashina *et al.*, 2017*b*; Grigoriev *et al.*, 2020) and HeLa nuclei (Iashina *et al.*, 2019; Iashina & Grigoriev, 2019; Grigoriev *et al.*, 2020) have been examined by both SANS and SESANS to scan their structure at all levels of chromatin organization. These investigations resulted in a new hypothesis about the universal principle of bi-fractal organization of interphase chromatin: with a *logarithmic* fractal structure on the larger scale and a *mass* fractal structure on the smaller scale.

Reported for the first time by Lebedev *et al.* (2005) for chromatin in chicken erythrocyte nuclei, the Q dependence of SANS intensity [$Q = (4\pi/\lambda)\sin(\theta/2)$, where θ is the scattering angle and λ is the wavelength of the incident radiation] is well described by the power function $I(Q) = Q^{-\nu}$, with the exponent $\nu = 2.4$ at the scale of 15–400 nm, and $\nu = 2.9$ (*i.e.* close to 3) at the scale from 400 to 1500 nm. An exponent close to 3 was interpreted as a special type of matter organization – the logarithmic fractal (Iashina & Grigoriev, 2017; Iashina *et al.*, 2017*b*, 2019). Independent SESANS measurements give the spin-echo correlation function, which is well described by the exponential decay $G(z) = \exp(-z/\xi)$ with the correlation length $\xi = 3700$ nm in a range of spin-echo length z from 300 nm to 12 000 µm. Both experimental dependences describing the large-scale organization of chromatin in a chicken erythrocyte nucleus (a cubic law in SANS intensity and an exponential decay in SESANS correlation function) reflect the nature of the structural organization of chromatin in the nucleus of a living cell, which corresponds to a logarithmic correlation function on scales from 400 to 3700 nm (the size of the nucleus) (Iashina *et al.*, 2017*b*).

In order to support the general hypothesis of the bi-fractal structure of chromatin in interphase nuclei, a SANS study has recently been performed on interphase HeLa nuclei with the momentum transfer ranging from the nucleosome size (∼10 nm) to the nucleus size (∼6000 nm) (Iashina *et al.*, 2019). It was shown that the small-scale structure corresponds to a mass fractal with dimension $D_F = 2.4$ at the scale from 9 to 80 nm. The large-scale organization corresponds to a logarithmic fractal ($\nu = 3$) at the scale from 80 to 5100 nm. The detected exponents for the HeLa nuclei are similar to those from chicken erythrocyte nuclei (Iashina *et al.*, 2017*b*, 2019). The SESANS correlation function also demonstrated exponential decay, $G(z) = \exp(-z/\xi)$, with $\xi = 5100$ nm in a range of z from 300 nm to 16 µm, confirming the logarithmic fractal structure of the large-scale organization of chromatin in HeLa nuclei.

Similarly, SANS measurements demonstrated the bi-fractal nature of chromatin structural organization in a rat lymphocyte nucleus (Iashina *et al.*, 2021). Surprisingly, the mass fractal structure is poorly developed in these nuclei, with the fractal dimension $D_F = 2.3$, and is limited in size to 60 nm. The logarithmic fractal was demonstrated to cover an extremely extensive range, from 60 to approximately 6000 nm.

In this work, the organization of chromatin in a biological cell nucleus was studied by the time-of-flight (ToF) SESANS method for the first time. The ToF method implies the wavelength dependence of the detected SESANS signal, which is different from the classical monochromatic SESANS technique. We show that the ToF-SESANS polychromatic method is better suited to the study of the structure of a biological sample on the micrometre scale than the monochromatic mode. The SESANS correlation function of the rat lymphocyte nucleus obtained from the experimental data is well described by an exponential decay that corresponds to the logarithmic fractal structure of the large-scale organization of chromatin. This conclusion confirms the findings obtained on a standard SANS machine, the beamline KWS-2 (MLZ, Munich, Germany), and on a very small angle scattering instrument with a focusing mirror, beamline KWS-3 (MLZ, Munich, Germany) (Iashina *et al.*, 2021).

The paper is organized in the following way. Section 2 presents descriptions of the sample preparation, experimental SESANS principles and the concept of SESANS from fractal objects. The experimental details of rat lymphocyte nuclei studied in ToF mode are presented in Section 3. The treatment of the data obtained is given in Section 4. Finally, the interpretation of the results and our conclusions are given in Sections 5 and 6, respectively.

2. Materials and methods

2.1. Sample preparation

The rat lymphocytes were isolated from rat spleen by mechanical treatment and placed in Versene solution [phosphate-buffered saline (PBS) with 3 m*M* ethylenediamine tetraacetic acid]. The resulting suspension of lymphocytes in Versene solution was carefully layered on 5 ml of sterile Ficoll (the density was 1.130 g cm^{-3}) and centrifuged for 15 min at 170 r min^{-1}. A layer of lymphocytes was transferred with a pipette into a test tube with a serum-free nutrient medium. The obtained lymphocytes were washed twice in Versene solution by centrifugation to remove the Ficoll completely. The resulting spleen cells were lysed for 5 min with 0.1% Triton-X100 in DMEM/F12 culture medium with 15 m*M* HEPES buffer [4-(2-hydroxyethyl)-1-piperazineethanesulfonic

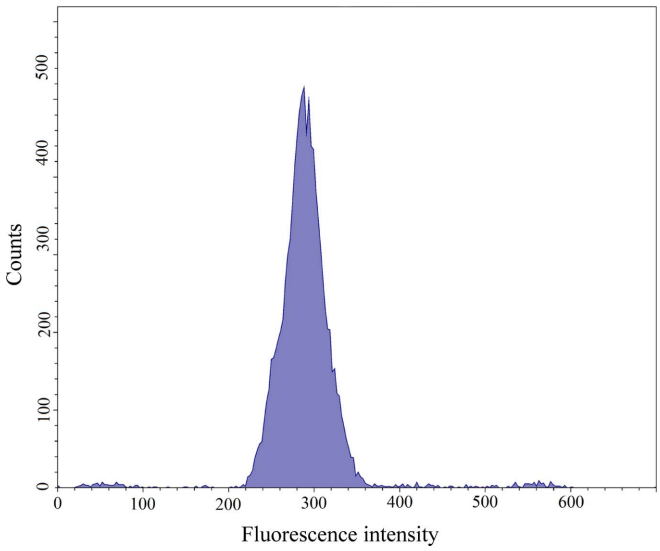

Figure 1
A flow cytometry histogram for the sample of rat lymphocyte nuclei.

acid]. The nuclei were then fixed by 0.5% glutaraldehyde for 10 min and washed from glutaraldehyde by centrifugation. The resulting precipitate was resuspended in PBS.

To analyse the properties of the cell nuclei on a flow cytometer (Cell Lab QUANTA SC by Beckman Coulter), the nuclei were stained with Hoechst 33342 (Sigma) fluorescent dye at a concentration of 10 μg ml^{-1}. This dye binds exclusively to DNA in its native form along the minor groove. In our study, it was used at a saturation concentration. The fluorescence intensity is directly proportional to the amount of DNA in the nucleus. The histogram in Fig. 1 shows that the fluorescence intensity for all nuclei is the same, so we can conclude that there is no loss or destruction of DNA after the treatments used.

2.2. Spin-echo SANS principles

SESANS allows the study of inhomogeneities at scales from 20 nm up to 20 μm (Rekveldt, 1996). This method gives reliable information on the correlation length of the object, which sometimes cannot be determined using conventional SANS because of resolution limitations.

In the SESANS technique the phenomenon of Larmor precession of the neutron magnetic moment in a magnetic field is employed to decode the scattering angle in the interaction of neutrons with the particle (Rekveldt, 1996). The polarization of the neutron beam is measured as it passes through the sample. We perform a scan along the spatial coordinate z, which is perpendicular to the direction of the neutron beam and is called the spin-echo length (SE length):

$$z = \frac{C\lambda^2 BL\cot(\theta_0)}{2\pi}, \tag{1}$$

where C is a constant, λ is the neutron wavelength, θ_0 is the angle of inclination of the front and end faces of the precession devices towards the beam axis, B is the magnitude of the magnetic field in the precession device, and L is its length. The measured polarization $P(z)$ depends on the mesostructure of the sample and is described as

$$\begin{aligned}\frac{P}{P_0(z)} &= \exp\{l\sigma[G(z)-1]\}\\ &= \exp[l\sigma G(z)]\exp(-l\sigma)\\ &= \exp[l\sigma G(z)]\,P_\infty,\end{aligned} \tag{2}$$

where l is the thickness of the sample, σ is the total neutron cross section of the sample, P_0 is the initial polarization, $P_\infty = \exp(-l\sigma)$ is the saturation of polarization and $G(z)$ is the SESANS correlation function for the object. The SESANS correlation function $G(z)$ approaches zero for $z > 2\xi$, where ξ is the correlation length of the scatterer. The polarization signal reaches saturation at a large SE length z,

$$P/P_0(z)|_{z>2\xi} \simeq P_\infty. \tag{3}$$

It is very important to measure the polarization saturation value accurately in order to know σ and to extract the SESANS correlation function $G(z)$ unambiguously from the polarization signal [equation (2)].

As shown by Krouglov *et al.* (2003) for isotropic systems, the SESANS function $G(z)$ is connected to the spatial correlation function $\gamma(r) = \langle\int_{\mathbb{R}^3}\rho(\mathbf{r}')\,\rho(\mathbf{r}'+\mathbf{r})\,\mathrm{d}\mathbf{r}'\rangle$, where $\rho(\mathbf{r})$ is the scattering density of the sample and the angle brackets denote averaging over all orientations, via the Abel transformation (Andersson *et al.*, 2008)

$$G(z) = \frac{2}{\xi}\int_z^\infty \frac{\gamma(r)r}{(r^2-z^2)^{1/2}}\,\mathrm{d}r, \tag{4}$$

where ξ is the correlation length. The inverse Abel transformation is

$$\gamma(r) = -\frac{\xi}{\pi}\int_r^\infty \frac{G'(z)}{(z^2-r^2)^{1/2}}\,\mathrm{d}z. \tag{5}$$

The correlation function $\gamma(r)$ is the Fourier transform of the intensity of neutron scattering $I(Q)$ measured in the SANS experiment,

$$I(Q) = \frac{1}{2\pi}\int_0^\infty \gamma(r)\frac{\sin(Qr)}{Qr}\,r^2\,\mathrm{d}r. \tag{6}$$

The SESANS correlation function $G(z)$ is connected to the neutron scattering intensity of $I(Q)$ in the following way:

$$G(z) = \frac{1}{k_0^2\sigma}\int_{\mathbb{R}^2}\cos(zQ_z)\,I(Q)\,\mathrm{d}Q_y\,\mathrm{d}Q_z, \tag{7}$$

where k_0 is the neutron wavenumber, σ is the total scattering cross section and $\mathbf{Q} = (0, Q_y, Q_z)$ is the scattering vector. The Fourier–Abel–Hankel cycle relates the three functions $I(Q)$, $G(z)$ and $\gamma(r)$ to each other. All transformations are bijective, and if one of these functions is known, the others can be completely reconstructed (Andersson *et al.*, 2008).

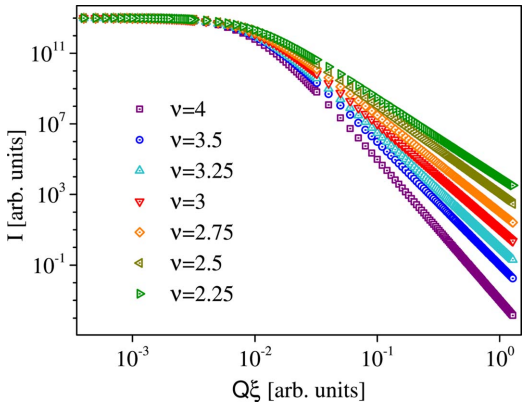

Figure 2
The scattering intensity $I(Q)$ described by equation (8) for different values of the exponent ν. The lowest curve shows scattering from the 3D non-fractal object ($\nu = 4$). Two curves slightly higher correspond to surface fractals ($\nu = 3.5$ and $\nu = 3.25$). The middle curve corresponds to an intermediate value of the parameter $\nu = 3$, *i.e.* the logarithmic fractal. The three upper curves correspond to volume fractals $\nu = 2.75$, $\nu = 2.5$ and $\nu = 2.25$.

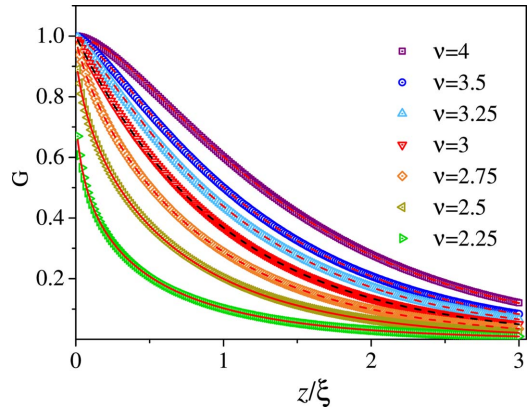

Figure 3
The SESANS correlation function $G(z)$ for different values of the exponent ν. The highest curve shows scattering from the 3D non-fractal object ($\nu = 4$). The two slightly lower curves correspond to surface fractals with $\nu = 3.5$ and $\nu = 3.25$. The middle curve corresponds to an intermediate value of the parameter $\nu = 3$, *i.e.* to the logarithmic fractal. The three lower curves correspond to volume fractals ($\nu = 2.75$, $\nu = 2.5$ and $\nu = 2.25$). The dashed lines are fitting curves consisting of elementary functions [equation (12)] that approximate the expression for the spin-echo correlation function of the fractal particle [equation (11)].

2.3. SESANS from fractal objects

The scattering intensity from fractal objects of a finite size with a correlation length ξ can be written in a general form as

$$I(Q) \simeq \frac{1}{[1+(\xi Q)^2]^{\nu/2}}, \tag{8}$$

where ν is an exponent associated with the fractal dimension. The SAS method introduces the classification of fractal objects through the value of the exponent ν (Teixeira, 1988). It identifies scattering by three-dimensional nonfractal particles as being well described by equation (8) with $\nu = 4$. The deviation of ν from 4 indicates the fractal structure of the particle: $4 > \nu > 3$ for a surface fractal and $3 > \nu > 2$ for a mass (or volume) fractal. The intermediate case with $\nu = 3$ between mass and surface fractals is identified as a special case of the logarithmic fractal (Iashina *et al.*, 2017*b*). Fig. 2 shows the scattering intensity from fractal objects [equation (8)] with different values of the exponent ν versus $Q\xi$.

The SESANS correlation function of a fractal object is the Hankel transform [equation (7)] of the scattering intensity [equation (8)],

$$G(z) = \frac{1}{k_0^2 \sigma} \int_{\mathbb{R}^2} \cos(zQ_z) \frac{A}{[1+(\xi Q)^2]^{\nu/2}} \, \mathrm{d}Q_y \, \mathrm{d}Q_z. \tag{9}$$

The constant A can be found by normalization of the scattering cross section,

$$\sigma = \frac{2\pi A}{k_0^2} \int_{\mathbb{R}} \frac{\mathrm{d}Q}{[(Q\xi)^2+1]^{\nu/2}} = \frac{2\pi A}{\xi^2 k_0^2} \frac{1}{(\nu-2)}. \tag{10}$$

The details of the integration of equation (9) are presented by Iashina & Grigoriev (2017). After integration and normalization procedures the expression for the SESANS correlation function of a fractal object is given by

$$G(z) = \frac{2}{\Gamma[(\nu/2)-1]} \left(\frac{z}{2\xi}\right)^{(\nu/2)-1} K_{(\nu/2)-1}\left(\frac{z}{\xi}\right), \tag{11}$$

where $\Gamma(n)$ is the Gamma function and $K_n(z/\xi)$ is the MacDonald function. Fig. 3 shows the SESANS correlation function of a fractal object [equation (9)] with different indices ν versus z/ξ.

The expression for $G(z)$ given by special functions can be approximated by a combination of elementary functions (details given in Appendix *A*),

$$G(z) = \frac{\pi^{1/2}}{\Gamma[(\nu/2)-1]} \left\{ \frac{z+a_0}{2\xi} \left[1 + \frac{\xi}{2(z+a_0)} \right] \right\}^{(\nu-3)/2} \exp(-z/\xi), \tag{12}$$

where ξ and a_0 are, respectively, the upper and lower limits of the fractal. The approximate expression [equation (12)] follows the curves given by the exact expression [equation (11)] extremely well.

The dashed lines in Fig. 3 correspond to equation (12) with the best fitted parameters (ν and ξ). As a result of the approximation, the value of ν coincides with its given value within an accuracy of a few per cent, and the parameter ξ for each curve is equal to 1 with high accuracy.

Thus, in the above consideration, we have demonstrated that fractal objects of a finite size from a_0 to ξ can be studied by SESANS, similarly to SANS. The experimentally measured function $G(z)$ and the parameters ν and ξ can be found from the best fit.

3. ToF-SESANS study of biological nuclei

3.1. ToF-SESANS study of rat lymphocyte nuclei

The SESANS study of the structural organization of chromatin from rat lymphocyte nuclei was carried out in the range

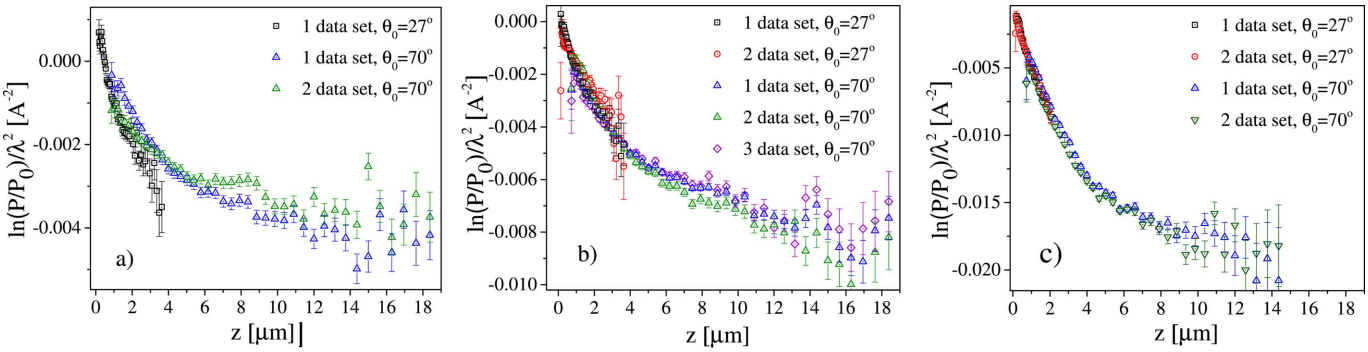

Figure 4
Normalized SESANS signal $\ln(P/P_0)/\lambda^2$ versus SE length z obtained from rat lymphocyte nuclei measured at different sample thicknesses, (*a*) 1 mm, (*b*) 2 mm and (*c*) 5 mm. The experiments were performed with poleshoe angles $\theta_0 = 27°$ (SE length range 1.5×10^2 to 3.5×10^3 nm) and $\theta_0 = 70°$ (SE length range 3.5×10^3 to 1.9×10^4 nm).

of SE lengths 1.5×10^2 to 1.9×10^4 nm on the LARMOR instrument at ISIS. LARMOR uses a white neutron beam from Target Station 2 with a wavelength range of 0.3–1.3 nm. The nuclei were put in a solution of $D_2O > 95\%$ to reach the maximum scattering contrast between the chromatin and the buffer.

The measurements on rat lymphocyte nuclei were carried out with two different configurations of the precession devices to cover a wide range of SE lengths: with the poleshoe angle $\theta_0 = 27°$ to obtain SE lengths $z = 1.5 \times 10^2$ to 3.5×10^3 nm, and with $\theta_0 = 70°$ to obtain SE lengths $z = 3.5 \times 10^3$ to 1.9×10^4 nm. SESANS measurements at two different θ_0 are analogous to SANS measurements with different sample-to-detector distances (2 or 10 m), aiming to provide a wide Q range. All measurements were made twice and then averaged to obtain a signal that is more statistically resolved. The measurements were made for three different thicknesses of the sample, 1 mm [Fig. 4(*a*)], 2 mm [Fig. 4(*b*)] and 5 mm [Fig. 4(*c*)].

The repeated measurements of the same curve $P(z)$ at two different poleshoe angles θ_0 and for three different thicknesses of the sample are justified by a search for the best statistics of the signal in the 'corresponding' range of the SE length z. The range of SE length z depends on the poleshoe angles θ_0 and the range of neutron wavelengths used. The best statistics of measurements related to the sensitivity of the technique are directly linked to the thickness of the sample and the total neutron scattering cross section which, in turn, is λ^2 dependent. The total neutron scattering cross section σ can be written as a function of λ^2 as $\sigma = \sigma_0\lambda^2$, where σ_0 is a constant. The sensitivity of SESANS has a dynamic range of just two orders of magnitude. It should not be under- or overestimated in terms of the measured polarization. The criteria for the best set of parameters of the SESANS instrument for a given sample are given in detail in Section 4.

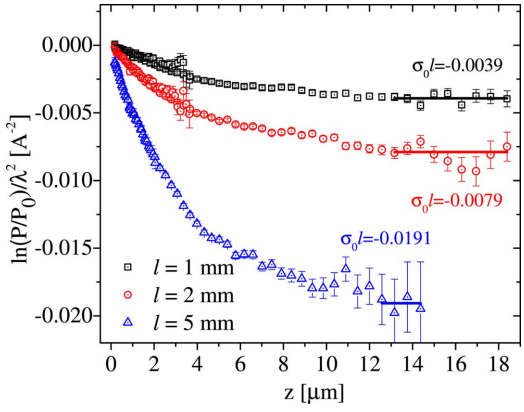

Figure 5
SESANS polarization $\ln(P/P_0)/\lambda^2$ as a function of SE length z from rat lymphocyte nuclei. Measurements were made with samples of 1 mm, 2 mm and 5 mm thickness.

One of the data sets at 1 mm sample thickness and $\theta_0 = 27°$ shows oscillatory (unstable) behaviour as a function of SE length z because of the low sensitivity of the spin-echo signal in a small SE length z and the small thickness of the weakly scattering sample. It was removed from the data treatment.

The data sets taken for the sample of thickness $l = 1$ mm [Fig 4(*a*)] demonstrate a common tendency for decay with increasing z. However, all three data sets differ from each other by 10–20% at some values of z, reflecting the low sensitivity of the spin-echo technique under the condition of limited instrument stability. The data sets taken for $l = 2$ mm [Fig 4(*b*)] are better merged, although the sets at $\theta_0 = 27°$ deviate somewhat from those taken at $\theta_0 = 70°$. All sets taken for $l = 5$ mm [Fig 4(*c*)] fit ideally with each other.

The results after averaging and merging the data collected for different configurations of the precession devices are presented in Fig. 5. The data demonstrate decay with increasing SE length z, resulting in the saturation level $\sigma_0 l$ being equal to -0.0039 ± 0.0003 for $l = 1$ mm, -0.0079 ± 0.0003 for $l = 2$ mm and -0.0191 ± 0.0003 for $l = 5$ mm. Determining the saturation level is important for correct extraction of the SESANS correlation function.

3.2. Sensitivity of SESANS signal: comparison of ToF and monochromatic modes.

The possibilities for extracting the SESANS correlation function $G(z)$ are limited due to the weak neutron scattering

attributed to cell nuclei. In addition to instrumental and statistical errors, the sensitivity of SESANS measurement depends on two factors: first, the saturation level of polarization P_∞ must be established, and second, the difference $P(0) - P_\infty$ must be as large as possible (once the first condition is met). The difference $P(0) - P_\infty$ is an analogue of the dynamic range that is often used in the context of signals, like sound and light. The larger the difference $P(0) - P_\infty$ (the larger the dynamic range), the more detailed the real SESANS signal [the spin-echo correlation function $G(z)$] will be.

The SESANS correlation function $G(z)$ can be definitely determined from the measured function $P/P_0(z)$ using equation (2). If the saturation level of the polarization P_∞ is not well defined, the SESANS correlation function $G(z)$ cannot be reconstructed at all from the measured function $P/P_0(z)$. Thus, it is essential to establish the saturation level in SESANS measurements.

The saturation level of polarization can be varied by varying the sample thickness l or the total scattering cross section σ. For a SESANS instrument operating at one wavelength only (say, $\lambda = 2$ Å), we have just one option: varying the thickness of the sample.

It is often insufficient to measure a few millimetres of sample to determine the saturation level. The maximum thickness of a sample that can be measured in an experiment is 10 mm, which corresponds to a sample volume of the order of 1 cm^3. However, such a volume of a biological sample is too large and is extremely difficult to provide. Moreover, to measure a 10 mm thick sample is technically difficult, since the measurement would be hampered by the low transmission through a sample filled with hydrogen, as is typical for a biological sample. Thus, biological samples are simultaneously characterized by a weak neutron coherent scattering cross section and a relatively high incoherent diffuse scattering cross section, resulting in low transmission. To get around these difficulties one has to vary the neutron wavelength and use a polychromatic neutron beam.

In other words, since it is impossible to increase the thickness of the specimen l, one should change the other parameter, σ, which can be easily done via variation of the neutron wavelength λ. The total cross section for SANS depends on the wavelength as λ^2. Therefore a variation in the wavelength from $\lambda = 2$ Å to $\lambda = 12$ Å will result in a change in σl by 36 times. In our previous work (Iashina *et al.*, 2017*a*) we discussed the necessity of being able to change the neutron wavelength in a SESANS experiment. This is important in the case of weakly scattering samples such as biological objects, in particular in the case of biological cell nuclei.

In contrast to the monochromatic SESANS method where the SE length z is varied by the magnetic field B, in ToF-SESANS z is altered by the neutron wavelength λ, as the SE length z is proportional to λ^2 [equation (1)]. As a result, long-wavelength neutrons play the major part in measurements at a large SE length z (on LARMOR at ISIS this can be up to 13 Å). The total small-angle scattering cross section is increased simultaneously and linearly with the increase in SE length z. This means that the saturation level of the polarization can be measured even with small sample thicknesses (Figs. 2 and 3).

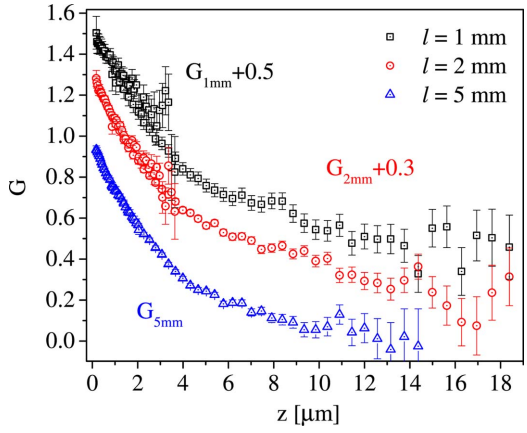

Figure 6
SESANS polarization G as a function of SE length z from rat lymphocyte nuclei for sample thicknesses $l = 1$ mm, $l = 2$ mm and $l = 5$ mm.

Although the sensitivity of the SESANS signal increases together with the difference $P(0) - P_\infty$, the precision of the polarization measurement has some physical limitations related to the limited stability of the magnetic field. Every experimental point in the SESANS signal is measured with a systematic error $\delta_z > 0.01$ (flipper efficiency < 99%). In reality this error is larger than 1%, and therefore the value of P_0 should not be smaller than 0.1 since its error bars exceed the value of 0.01. The sensitivity of the SESANS signal varies with the thickness of the sample. The precision of extracting the SESANS correlation function $G(z)$ from $\ln(P/P_0)/\lambda^2$ is defined by the dynamic range $P(0) - P_\infty$.

3.3. Spin-echo correlation function $G(z)$

The SESANS correlation function $G(z)$ is extracted from the polarization signal $\ln(P/P_0)/\lambda^2$. Fig. 6 shows the SESANS correlation functions $G(z)$ measured with sample thicknesses of 1 mm (black squares), 2 mm (red circles) and 5 mm (blue triangles). The measurement accuracy increases noticeably with increasing sample thickness. The error bars in the curve for the 5 mm thick sample do not exceed 2%, while for the 1 mm thick sample they are of the order of 10%.

4. Results

The fractal model presented in Section 2.3 was applied to the SESANS data shown in Fig. 6. The SESANS correlation functions $G(z)$ obtained from the rat lymphocyte nuclei with different sample thicknesses were fitted using equation (12).

Fig. 7 presents the experimental SESANS correlation function G as a function of the SE length z (black open triangles) that was approximated by equation (12) (red line) with best fitted parameters $\nu = 3.5 \pm 0.1$ and $\xi = 3.0 \pm 0.2$ μm. The fitting curve does not completely match the experimental data at small SE lengths z since the experimental data are too noisy in this range. At the same time, this range of z is very important and in practice determines the parameter ν which

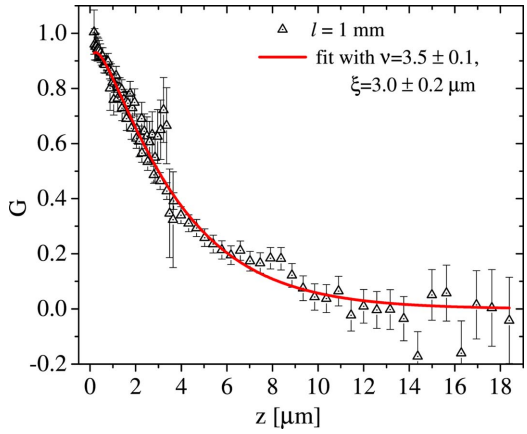

Figure 7
The SESANS correlation function G as a function of SE z from rat lymphocyte nuclei measured in 1 mm thick cuvette. Open black triangles are experimental data and the red line is the fitting curve obtained using equation (12) with parameters $\nu = 3.5 \pm 0.1$ and $\xi = 3.0 \pm 0.2$ μm.

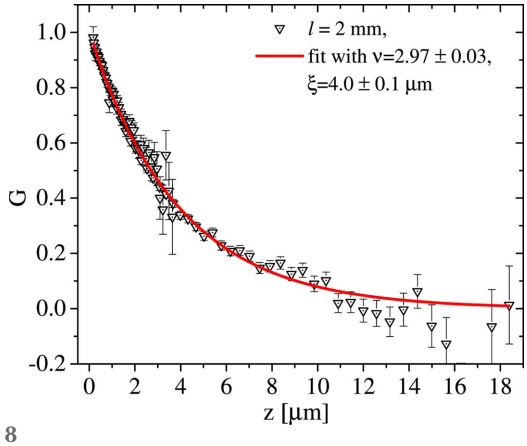

Figure 8
The SESANS correlation function G as a function of SE length z from rat lymphocyte nuclei measured in a 2 mm thick cuvette. Open black triangles are experimental data and the red line is the fitting curve obtained using equation (12) with parameters $\nu = 2.97 \pm 0.03$ and $\xi = 4.0 \pm 0.1$ μm.

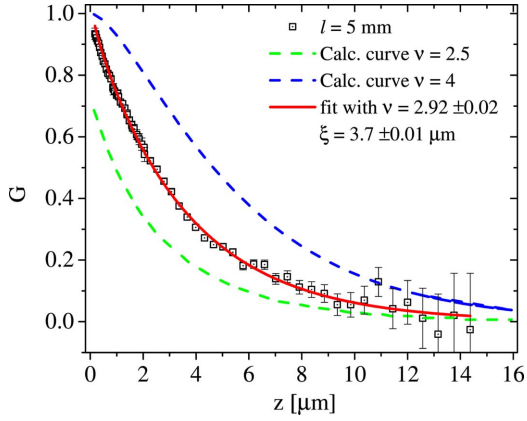

Figure 9
The SESANS correlation function G as a function of SE length z from rat lymphocyte nuclei measured in a 5 mm thick cuvette. Open black squares are experimental data and the red line is the fitting curve obtained using equation (12) with parameters $\nu = 2.92 \pm 0.02$ and $\xi = 3.7 \pm 0.1$ μm. The dashed lines are the curves obtained with (blue) $\nu = 4$ and $\xi = 3.7$ μm and (green) $\nu = 2.5$ and $\xi = 3.7$ μm.

characterizes the fractal dimension. For this reason, one needs to perform very precise measurements of the SESANS correlation function $G(z)$ in the range of small z.

The precision of the measurements improves in the case of the sample of 2 mm thickness. Fig. 8 presents the SESANS correlation function $G(z)$ that is approximated by equation (12) with best fitting parameters $\nu = 2.97 \pm 0.03$ and $\xi = 4.0 \pm 0.1$ μm.

The best precision in the SESANS measurements is reached in the case of the sample of 5 mm thickness (Fig. 9). The best fitted parameters of the approximated curve [equation (12)] are $\nu = 2.92 \pm 0.02$ and $\xi = 3.7 \pm 0.1$ μm.

The approximation procedure for the SESANS correlation function [equation (11)] with $\nu = 3$ can be considerably simplified, as the theoretical expression for $G(z)$ can be given as the exponential decay,

$$G(z) = \exp(-z/\xi). \tag{13}$$

It was shown earlier (Iashina *et al.*, 2017*b*; Iashina & Grigoriev, 2017) that exponential decay of the SESANS correlation function corresponds to the logarithmic correlation function (logarithmic fractal) which was previously detected using the cubic law of scattering intensity $I(Q) = Q^{-3}$ in SANS (Iashina *et al.*, 2021).

To see better the difference between a non-fractal object (blue dashed line), a logarithmic fractal (red line) and a volume fractal, for instance with $\nu = 2.5$ (green dashed line), we added the SESANS correlation functions of equation (11) with the correlation length $\xi = 3.7$ μm and $\nu = 4$ (non-fractal object) and $\nu = 2.5$ (volume fractal) to the SESANS correlation function of the logarithmic fractal (red line) in Fig. 9 for comparison.

5. Discussion

5.1. Logarithmic fractal model

The concept of the fractal organization of chromatin is considered as one of the most productive hypotheses to describe the inner nucleus structure, but it is not yet well established. SESANS experiments provide evidence of a logarithmic fractal structure for the large-scale organization of chromatin in rat lymphocyte nuclei (present study) and, previously, in chicken erythrocyte (Iashina *et al.*, 2017*b*) and HeLa nuclei (Iashina *et al.*, 2019). The SESANS measurements are excellently complemented and confirmed by SANS data (Iashina *et al.*, 2017*b*, 2019, 2021; Iashina & Grigoriev, 2019; Grigoriev *et al.*, 2020, 2021).

We propose a model of the logarithmic fractal in 3D space based on the principle of volume conservation upon the additive procedure of constructing the logarithmic fractal. The procedure of building a logarithmic fractal is presented in Fig. 10. We start with a cube of volume V (red). As a second step we have to add eight cubes of volume $V/8$ (yellow) to every corner of the red cube, then as the next step we have to add eight cubes of volume $V/64$ (green) to every corner of every cube of the previous iteration (yellow cubes) and so on.

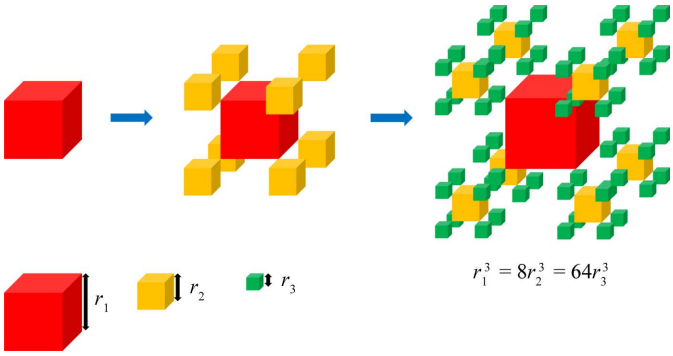

Figure 10
The 3D logarithmic fractal model based on the volume-conserving principle.

The law of volume conservation for this additive procedure can be written as the following recurrence relation:

$$r_1^3 = 2^3 \times r_2^3 = 2^{3\times 2} r_3^3 = 2^{3(n-1)} r_n^3 = V_n = V. \qquad (14)$$

The linear size (side) of the cube at each subsequent iteration is halved. The total volume of the cubes in each iteration is the same and equal to V, the volume of the first cube. The logarithmic fractal of the third generation is presented on the right-hand side of Fig. 10. We see that elements (cubes) of different sizes are homogeneously distributed in space.

Computer modelling of the SANS experiment on the 3D logarithmic fractal presented in Fig. 10 shows a power law of scattering intensity proportional to Q^{-3}, which is equivalent to the results of real experiments on the organization of chromatin (manuscript in preparation). The cubic dependence, as shown above, corresponds to the logarithmic correlation function $\gamma(r) = \ln(r/\xi)$ for $r < \xi$ and to the exponential decay of the SESANS correlation function $G(z) = \exp(-z/\xi)$. This illustration is a preliminary model of the logarithmic fractal that satisfies its principles and the exponential decay in the SE length dependence in the SESANS data. A real picture of the organization of chromatin in a biological cell has local features of structure and deserves a separate deep and comprehensive study.

5.2. ToF-SESANS for chromatin organization in a nucleus

The possibilities for extracting the SESANS function $G(z)$ appear to be limited in the case of weak neutron scattering. For monochromatic SESANS with only one wavelength of the incident neutron beam, measurements might be possible in the range of large z, where the measured polarization reaches its saturation polarization level. For smaller z the sensitivity of the instrument would not allow the extraction of any reasonable data. Thus, the range of SE length z will be considerably limited, to the extent of hiding information on the inner structure of the object. This limitation is due not to statistical errors in neutron measurements but to the lack of stability of many devices used to manipulate the orientation of neutron spin in a SESANS instrument. This instability means that the polarization in the spin-echo instrument cannot be measured to better than 1%.

This limitation can be overcome if one is able to vary not only the thickness of the sample l but also the total neutron cross section via the neutron wavelength. The cross section for SANS depends on the wavelength as λ^2. Therefore a change in wavelength from $\lambda = 3$ Å to $\lambda = 13$ Å will change the sensitivity of the SESANS method by 25 times in one measurement. This variation in the neutron wavelength is naturally imposed in the ToF-SESANS method.

For fractal objects the SESANS method is applied to measure the structure of particles ranging in size from 100 nm to 10 µm. To obtain the necessary information we used a wide wavelength range that considerably increases the sensitivity of the SESANS signal to weak neutron scattering. We also used three different thicknesses of the sample to extract information, over a range from small z with a large thickness to large z with a small thickness.

In general, in order to cover fully the two decades from 100 nm to 10 µm in measurements of the SESANS function $G(z)$, one must perform such ToF-SESANS measurements with at least two different sample thicknesses and over a wide neutron wavelength range. Such a SESANS measurements protocol is analogous to the protocol for SANS measurements at three different sample-to-detector distances aiming to provide a wide Q range from 10^{-2} to 1 nm^{-1}.

Finally, we have showed the applicability of ToF-SESANS to study the inner fractal structure of the nuclei of biological cells. The advantage of studying such objects by SESANS is the relatively low dispersion in the sizes of the nuclei under study. A finite size of monodisperse particles in the sample is an obligatory condition for studies using the SESANS method.

6. Conclusion

In conclusion, we propose time-of-flight spin-echo small-angle neutron scattering as a highly applicable method of studying chromatin organization. Since there are a huge variety of biological cells, the ToF-SESANS instrument will be in demand from the biological community.

We have formulated a measurement protocol for biological cell nuclei using ToF-SESANS. The protocol implies measurement of two different thicknesses of the sample, provided that a wide range of incident neutron wavelengths are used. The applied method can be used to show the logarithmic fractal structure of the large-scale organization of chromatin. The correlation function of the rat lymphocyte nucleus changes for the logarithmic function $\gamma(r) = \ln(r/\xi)$ (ξ = 3.7 µm) on a scale from 0.1 to 3.7 µm. We suppose that such a structure of rat lymphocyte nuclei provides a high accessibility of proteins and enzymes to a specific gene site and results in fast diffusion of functional proteins.

We believe that this knowledge can help in building a correct model of chromatin that will connect the structure with the function and explain how biological processes work in nuclei.

APPENDIX A

To approximate the expression for $G(z)$ given by special functions through a combination of elementary functions, we consider the following integral representation for the MacDonald function (Gradshteyn & Ryzhik, 2014),

$$K_\nu(x) = \left(\frac{\pi}{2x}\right)^{1/2} \frac{\exp(-x)}{\Gamma(\nu+1/2)} \int_0^\infty \exp(-t)\, t^{\nu-1/2} \left(1+\frac{t}{2x}\right)^{\nu-1/2} \mathrm{d}t. \tag{15}$$

The behaviour of equation (15) was considered in two cases: when $x \to 0$ and for $x > 1/2$.

The first case, $x \to 0$, gives the following expression,

$$K_\nu(x) = \left(\frac{\pi}{2x}\right)^{1/2} \frac{1}{\Gamma(\nu+1/2)} \frac{1}{(2x)^{\nu-1/2}} \int_0^\infty \exp(-t)\, t^{2\nu-1}\, \mathrm{d}t = \frac{2^{\nu-1}\Gamma(\nu)}{x^\nu}. \tag{16}$$

The correlation function in this case is written as

$$G(z) \simeq \frac{2}{\Gamma[(D/2)-1]} (z/2\xi)^{(D/2)-1} \frac{2^{(D/2)-2}\Gamma[(D/2)-1]}{(z/\xi)^{(D/2)-1}} = 1. \tag{17}$$

Considering equation (15) when $x > 1/2$, the following expression was used:

$$K_\nu(x) = \left(\frac{\pi}{2x}\right)^{1/2} \exp(-x) \left[1 + \sum_{r=1}^{\infty} \frac{\Gamma(\nu+1/2-r)}{\Gamma(\nu+1/2)} \times \frac{(\nu-1/2)\ldots(\nu-r+1/2)}{r!} (2x)^{-r}\right]. \tag{18}$$

The expression in square brackets is a convergent power series of argument $1/(2x)$. The argument is smaller than 1. By cutting the series to the first term in equation (18), we will have the following expression:

$$K_\nu(x) \simeq \left(\frac{\pi}{2x}\right)^{1/2} \exp(-x)\left[1+\frac{1}{2x}(\nu-1/2)\right]. \tag{19}$$

The expression in equation (18) can be approximated by elementary functions using equation (19) and Taylor expansion of a function $(1+y)^\alpha \simeq 1+\alpha y$ for $y < 1$:

$$K_\nu(x) \simeq \left(\frac{\pi}{2x}\right)^{1/2} \exp(-x)\left[1+\frac{1}{2x}\right]^{(\nu-1/2)}. \tag{20}$$

The approximation of the SESANS correlation function $G(z)$ when $z/\xi > 1/2$ can be written as follows:

$$G(z) = \frac{\pi^{1/2}}{\Gamma[(\nu/2)-1]} \left[\frac{z}{2\xi}\left(1+\frac{\xi}{2z}\right)\right]^{(\nu-3)/2} \exp(-z/\xi). \tag{21}$$

The approximate expression of equation (21) describes the exact expression of equation (11) for all z/ξ except the range of small values of the argument. It is seen that for $\nu > 3$ and at $z = 0$, the SESANS function $G(0) = 0$, and for $\nu < 3$ and at $z = 0$, the SESANS function $G(0) = \infty$. Only at $\nu = 3$ and $z = 0$ does the SESANS function $G(0) = 1$, and equation (21) has no singular point and is equal to the decreasing exponent, which coincides with equation (11). To avoid this specific feature in the vicinity of zero, in equation (21) we introduce the additional parameter a_0 and the correct expression for equation (21) is

$$G(z) = \frac{\pi^{1/2}}{\Gamma[(\nu/2)-1]} \left\{\frac{z+a_0}{2\xi}\left[1+\frac{\xi}{2(z+a_0)}\right]\right\}^{(\nu-3)/2} \times \exp(-z/\xi). \tag{22}$$

From a physical viewpoint, this is quite justified, since fractals have a lower limit. Equation (21) can be used for data processing because the point $G(0)$ is impossible to measure in practice.

Acknowledgements

We would like to thank the ISIS Neutron Centre (Rutherford Appleton Laboratory, Didcot, Oxfordshire, UK) for the beamtime allocation. Author contributions: conceptualization, EI and SG; writing, EI and SG; sample preparation, EV, RP, RK and NF; investigation and formal analysis, EI, SG, CD, WB and RD; supervision, SG.

Funding information

The following funding is acknowledged: Russian Science Foundation (grant No. 20-12-00188).

References

Andersson, R., van Heijkamp, L. F., de Schepper, I. M. & Bouwman, W. G. (2008). *J. Appl. Cryst.* **41**, 868–885.

Boettiger, A. N., Bintu, B., Moffitt, J. R., Wang, S., Beliveau, B. J., Fudenberg, G., Imakaev, M., Mirny, L. A., Wu, Ch. & Zhuang, X. (2016). *Nature*, **529**, 418–422.

Bouwman, W. G., Duif, C. P., Plomp, J., Wiedenmann, A. & Gähler, R. (2011). *Physica B*, **406**, 2357–2360.

Gradshteyn, I. S. & Ryzhik, I. M. (2014). *Table of Integrals, Series, and Products*, 8th ed. Cambridge: Academic Press.

Grigoriev, S. V., Iashina, E. G., Bairamukov, V. Y., Pipich, V., Radulescu, A., Filatov, M. V., Pantina, R. A. & Varfolomeeva, E. Y. (2020). *Phys. Rev. E*, **102**, 032415.

Grigoriev, S. V., Iashina, E. G., Wu, B., Pipich, V., Lang, C., Radulescu, A., Bairamukov, V. Y., Filatov, M. V., Pantina, R. A. & Varfolomeeva, E. Y. (2021). *Phys. Rev. E*, **104**, 044404.

Halverson, J. D., Smrek, J., Kremer, K. & Grosberg, A. Y. (2014). *Rep. Prog. Phys.* **77**, 022601.

Iashina, E. G., Bouwman, W. G., Duif, C. P., Filatov, M. V. & Grigoriev, S. V. (2017*a*). *J. Phys. Conf. Ser.* **862**, 012010.

Iashina, E. G., Filatov, M. V., Pantina, R. A., Varfolomeeva, E. Yu., Bouwman, W. G., Duif, C. P., Honecker, D., Pipich, V. & Grigoriev, S. V. (2019). *J. Appl. Cryst.* **52**, 844–853.

Iashina, E. G. & Grigoriev, S. V. (2017). *J. Surf. Investig.* **11**, 897–907.

Iashina, E. G. & Grigoriev, S. V. (2019). *J. Exp. Theor. Phys.* **129**, 455–458.

Iashina, E. G., Varfolomeeva, E. Y., Pantina, R. A., Bairamukov, V. Y., Kovalev, R. A., Fedorova, N. D., Pipich, V., Radulescu, A. & Grigoriev, S. V. (2021). *Phys. Rev. E*, **104**, 064409.

Iashina, E. G., Velichko, E. V., Filatov, M. V., Bouwman, W. G., Duif, C. P., Brulet, A. & Grigoriev, S. V. (2017*b*). *Phys. Rev. E*, **96**, 012411.

Krouglov, T., de Schepper, I. M., Bouwman, W. G. & Rekveldt, M. T. (2003). *J. Appl. Cryst.* **36**, 117–124.

Krueger, S. (2022). *Curr. Opin. Struct. Biol.* **74**, 102375.
Lebedev, D. V., Filatov, M. V., Kuklin, A. I., Islamov, A. K., Kentzinger, E., Pantina, R., Toperverg, B. P. & Isaev-Ivanov, V. V. (2005). *FEBS Lett.* **579**, 1465–1468.
Lieberman-Aiden, E., van Berkum, N. L., Williams, L., Imakaev, M., Ragoczy, T., Telling, A., Amit, I., Lajoie, B. R., Sabo, P. J., Dorschner, M. O., Sandstrom, R., Bernstein, B., Bender, M. A., Groudine, M., Gnirke, A., Stamatoyannopoulos, J., Mirny, L. A., Lander, E. S. & Dekker, J. (2009). *Science*, **326**, 289–293.
Mahieu, E. & Gabel, F. (2018). *Acta Cryst.* D**74**, 715–726.
Mirny, L. A. (2011). *Chromosome Res.* **19**, 37–51.
Rekveldt, M. T. (1996). *Nucl. Instrum. Methods Phys. Res. B*, **114**, 366–370.
Stuhrmann, H. B. & Miller, A. (1978). *J. Appl. Cryst.* **11**, 325–345.
Svergun, D. I., Koch, M. H., Timmins, P. A. & May, R. P. (2013). *Small-Angle X-ray and Neutron Scattering from Solutions of Biological Macromolecules.* Oxford University Press.
Teixeira, J. (1988). *J. Appl. Cryst.* **21**, 781–785.